Design of an experimental platform for hybridization of atomic and superconducting quantum systems

Alessandro Landra,[1] Christoph Hufnagel,[1] Lim Chin Chean,[1] Thomas Weigner,[1,2,3] Yung Szen Yap,[1,4] Long Hoang Nguyen,[2] and Rainer Dumke[1,2,*]

[1]*Centre for Quantum Technologies, National University of Singapore, 3 Science Drive 2, Singapore 117543, Singapore*

[2]*Division of Physics and Applied Physics, Nanyang Technological University, 21 Nanyang Link, Singapore 637371, Singapore*

[3]*Atominstitut TU Wien, Stadionallee 2, Vienna 1020, Austria*

[4]*Faculty of Science and Centre for Sustainable Nanomaterials (CSNano), Universiti Teknologi Malaysia, 81310 UTM Johor Bahru, Johor, Malaysia*

(Received 22 March 2019; published 28 May 2019)

Hybrid quantum systems have the potential of mitigating current challenges in developing a scalable quantum computer. Of particular interest is the hybridization between atomic and superconducting qubits. We demonstrate an experimental setup for transferring and trapping ultracold atoms inside a millikelvin cryogenic environment, where interactions between atomic and superconducting qubits may be established, paving the way for hybrid quantum systems. We prepare ^{87}Rb atoms in a conventional magneto-optical trap and transport them via a magnetic conveyor belt into a UHV compatible dilution refrigerator with optical access. We store 5×10^8 atoms with a lifetime of 794 s in the vicinity of the millikelvin stage.

DOI: 10.1103/PhysRevA.99.053421

I. INTRODUCTION

Quantum technologies promise a new era in many existing applications, like computation [1–6], analog and digital quantum simulation [7–13], communication [14–16], and sensing [17]. Today, quantum states have been realized in many different physical systems like atoms [18], solid states [19], and photonic devices [20]. An important step in future quantum technologies is the creation of coherent interfaces between these systems, which will benefit from the combined advantages of each quantum system in an integrated device [21–23].

A particularly interesting hybrid quantum device is the combination of superconducting (SC) quantum circuits and ultracold atoms. Superconducting qubits [19] are widely considered to be among the most mature approaches for quantum computing. They are robust, are flexible in design, and admit a fast processing of quantum states. Moreover, continuous improvements over the last decade pushed them into the error correction regime [24]. Yet, there are still many challenges that SC qubits are facing. Overall, coherence times of SC qubits are still limited and highly dependent on external factors like fabrication techniques [25]. This restricts their use as effective quantum memories. Another obstacle that SC qubits face is that they cannot be interfaced to optical photons directly, which sets severe limits on their long-distance networking capabilities [26]. Neutral atom qubits are able to compensate for most of these shortcomings. Coherence times of neutral atoms, particularly in cryogenic environments, are on the order of 10 s [27], about three orders of magnitude longer than in SC qubits. In addition, the states of atomic qubits can be transferred directly to optical photons [28]. Few experimental realizations for ultracold atoms in a cryogenic environment have been reported, however they were limited to 4 K and above base temperatures [29–36], which is not suitable for SC qubits integration. Here, we describe the realization of an experimental setup for studying hybrid quantum systems, made of ultracold atoms and superconducting circuits. In this hybrid system we can exploit the long coherence of the atomic states and the fast high-fidelity driving of logical operations of superconducting qubits. Moreover, with a suitable state preparation of the former and a careful engineering of the electromagnetic modes in the latter [37,38], we can investigate different coupling mechanisms. Theoretical protocols for this hybrid system have been proposed. The state transfer and controlled-NOT gate operation can be performed between the two species of qubit, while more complex experiments will allow the stabilization of the Rabi oscillation of the SC qubit, using atomic clock techniques with feedback control and quantum random access memory [39–46]. Two coupling scenarios are available. First is the collective coupling of the rubidium 87 clock states, $|5^2S_{1/2}, F = 1\rangle$ and $|5^2S_{1/2}, F = 2\rangle$, to a microwave cavity field at 6.835 GHz, which is simultaneously coupled to a SC qubit [47,48]. Similarly, the atoms can be excited to a Rydberg state with high principal quantum number, resulting in a strong electrical dipole coupling with the electric fringe field of a planar circuit [49,50], e.g., the capacitor of a charge or transmon qubit.

One of the technical challenges in realizing such a hybrid system is the effect of the environment on the superconducting qubits. Their coherence can be shortened or even destroyed when they are affected by stray magnetic fields or light, meaning that we need to carefully control and shield both factors when and where necessary.

*rdumke@ntu.edu.sg

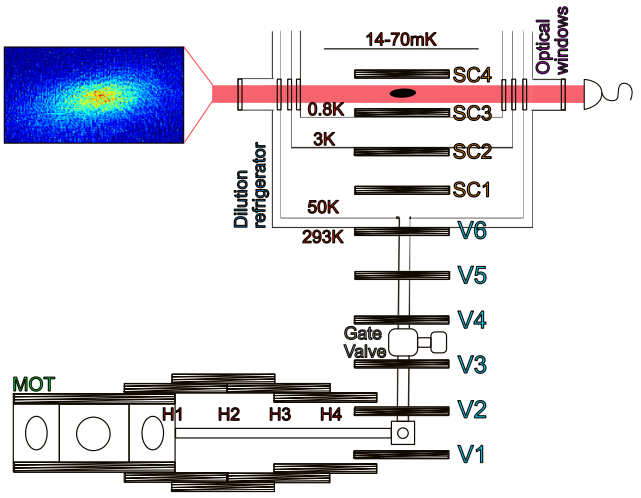

FIG. 1. Side view of the experimental setup. The atoms are loaded in the MOT through a Zeeman slower (missing in the schematics), from which a CF16 tube extends on the right side, called horizontal transport (H coils), at the end of which the vertical transport (V coils) starts, up to the cryostat (SC coils). Inset: Example of absorption imaging. The image is acquired through optical windows, available on two perpendicular axes.

In this paper we describe the experimental realization of a platform, suitable for the hybridization of SC and atomic qubits.

II. EXPERIMENTAL SETUP

We start the experiment by collecting 4×10^9 ^{87}Rb atoms from a Zeeman slower into a magneto-optical trap (MOT). After optical pumping to the $|F' = 2, m_F = +2\rangle$ state, 2×10^9 atoms are magnetically trapped in a quadrupole field with a gradient of 90 G/cm, at a temperature of 150 μK. We characterize the ultracold atoms by fluorescence imaging in the MOT chamber, and by absorption imaging in the cryostat. Lifetimes in the magnetic trap due to collisions with the background gas in the room-temperature (RT) vacuum chamber are typically 20 s.

The MOT chamber is connected with a CF16 vacuum tube to the cryostat, which is centered in the magnetic conveyor belt as shown in Fig. 1. The vacuum environment extends first horizontally (33.0 cm), then vertically (22.5 cm) up to the entrance of the bottom plate of a dry UHV compatible dilution refrigerator (DR). Inside the cryostat, the atoms move a further 17.5 cm vertically and pass through the 50-K shield, 3-K shield, and 800-mK shield (still shield). After the still shield the atoms approach the mixing chamber plate.

Along the vertical section, an all-metal gate valve separates the MOT and cryostat vacuum environments, to be able to detach the DR without breaking the room-temperature vacuum. Before the gate valve, a 5-L ion pump is attached to maintain the UHV inside the transport tube. The cryostat has a base temperature of 14 mK when the optical access is shielded. However, when the four CF40 windows are installed the temperature rises to 70 mK, due to the additional optical heat load. Inside the cryostat the atoms are held in a quadrupole magnetic trap in proximity to the millikelvin stage, which will later host the superconducting quantum circuit. The shield plates are equipped with mechanical shutters controlled externally in order to open and close a 12.5-mm hole for the passage of the atomic cloud. The shields are made of copper and aluminum, exhibiting very low resistivity at cryogenic temperatures, therefore the magnetic transport induces long lasting eddy currents. These eddy currents are reduced by slowing down the transport of the atoms (see Sec. III) and by radially segmenting the plates, starting from the center hole (eight segments each plate) following the optimization using finite element method simulation.

The magnetic conveyor belt [31] consists of 20 coils as shown in Fig. 1. The first pair of coils coincides with the MOT coils, and the horizontal transport is achieved with four additional pairs of coils in anti-Helmholtz configuration. At the 90° direction change, the vertical transport begins with six equally spaced coils that reach to the cryostat chamber. The vertical coils, casted in resin to eliminate eddy currents, have 40 windings each and are separated by 5 cm. Inside the cryostat, four superconducting coils, with 800 windings each, are anchored to the 3-K and still plates and wired to external current sources. The wiring consists of different sections. First the NbTi coil wire is soldered to a YBCO strip cladded in two copper layers and anchored to the shields. At the 3-K stage the YBCO strip is soldered to preinstalled high temperature superconductor lines reaching up to the external room-temperature feedthrough. We are able to drive 10 A on each line, without compromising the DR functionality. The room-temperature coils are powered by three car batteries in series, with current regulated by a parallel metal-oxide-semiconductor field-effect transistor based programmable proportional-integral-derivative controller, connected to unipolar and bipolar switches for each coil [51]. The superconducting coils are driven by four dedicated bipolar current sources controlled by analog signals.

In the cryostat stainless steel microwave lines have been installed. They are thermally anchored at each shield and they include attenuators, low-pass filters, circulators, and a high electron mobility transistor (HEMT) amplifier, sketched in Fig. 2. The current setup allows one to probe three-dimensional microwave cavities and SC qubits. We are currently using a rectangular cavity, in resonance with the atomic transition. The cavity is excited at its TE_{201} mode, allowing one to have atoms and SC qubits at the magnetic and electric field antinodes, respectively. A transversal through hole, 5 mm in diameter, has been drilled in the cavity, allowing the passage of the atoms, guided by superconducting electrodes. We have measured internal quality factors up to $Q_i = 5\times10^5$, and whenever the superconducting state is harmed by external fields we can use laser light to reset its original status.

III. METHODS

For the magnetic transport of cold atoms, two methods are typically applied. First, a pair of moving anti-Helmholtz coils can be used to transport the atoms with the shifting quadrupole field [52,53]. For this case the transport into a cryostat was realized in [32]. Second, a series of stationary overlapping

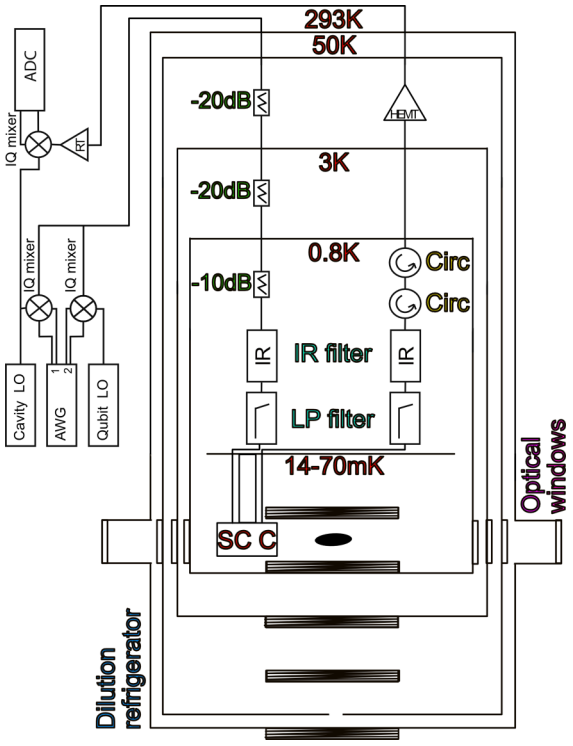

FIG. 2. Schematic of the room-temperature and cold microwave electronics for probing superconducting circuits. Attenuators, low-pass filters (LP filters), custom made IR filters, circulators (Circ), HEMT, and low noise room-temperature (RT) amplifiers have been installed. Superconducting quantum circuits (SC C) can be probed and measured with an arbitrary waveform generator (AWG), local oscillators (LO), and an analog to digital converter (ADC).

anti-Helmholtz coils can generate a moving quadrupole field by an appropriate current modulation [31,54]. The latter method was preferred, as there is no moving object involved, which will be an important condition upon entry of the atomic cloud into the cryostat.

The current pulses of each coil are calculated by fixing the trap geometry, which must allow a symmetry in two directions, whereas the remaining direction defines the transport axis. To simulate the current profiles for the horizontal transport, where x denotes the transport direction, we need to assume the following conditions [55]:

$$B(x_0) = 0 \quad \text{(at trapping position } x_0\text{)}, \tag{1}$$

$$\frac{\partial B_z}{\partial z}(x_0) = 120\ \text{G/cm}, \tag{2}$$

$$A = \frac{\partial B_y/\partial y}{\partial B_x/\partial x}(x_0) = \text{const}, \tag{3}$$

where A is the aspect ratio of the atomic cloud. Contributions to the magnetic field from three pairs of coils are necessary at each point in space to meet these three conditions. For the vertical transport, four coils should be used instead, except for the start and end of the transport, fulfilling the conditions

$$B(z_0) = 0 \quad \text{(at trapping position } z_0\text{)}, \tag{4}$$

$$\frac{\partial B_z}{\partial z(z_0)} = 120\ \text{G/cm}, \tag{5}$$

$$\frac{\partial^2 B_z}{\partial z^2_{z<z'}} = 0 \quad \text{(linear trapping gradient)}, \tag{6}$$

$$\sum_{i=1}^{4} I_i = 0, \tag{7}$$

where the third condition assures the trap has a linear gradient over a wide region defined by z' and the fourth requires the sum of the currents to be equal to zero, I_i denoting the current in each coil. Once the current profiles at each point of the transport have been generated, they need to be mapped into a time-dependent function $I_i(x, y, z) \to I_i(t)$. While performing the mapping, care must be taken to minimize jerk, in order to prevent heating of the atomic cloud. Moreover, when the cloud experiences changes in magnetic-field gradient along the path due to a mismatch in the simulated field and actual field, the cloud will heat up as well.

We need to define the equations of motion for space, velocity, and acceleration, with the necessary boundary conditions. The whole transport is ideally divided in three distinct

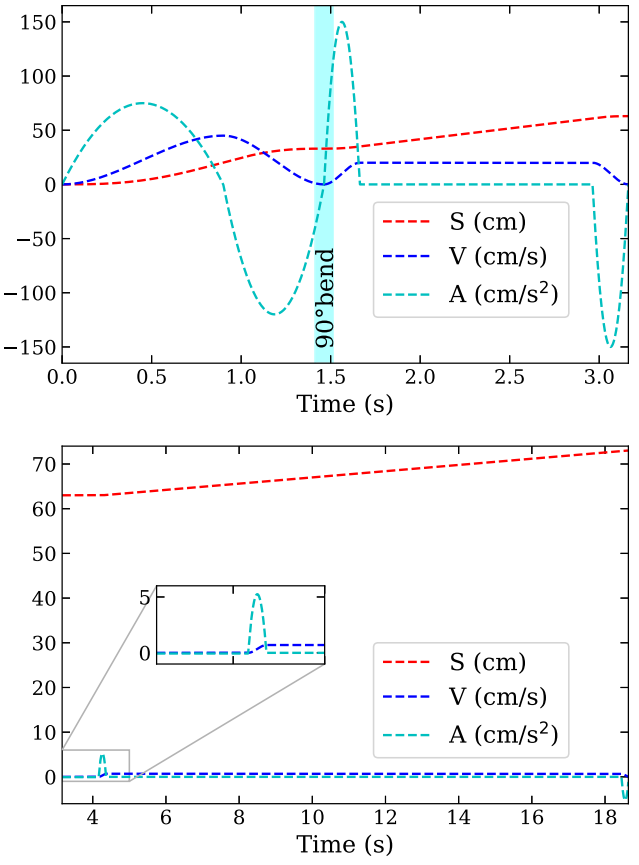

FIG. 3. Acceleration, velocity, and position profiles of the magnetic transport. The first two sections are in the upper plot; the last section is plotted below with a different timescale.

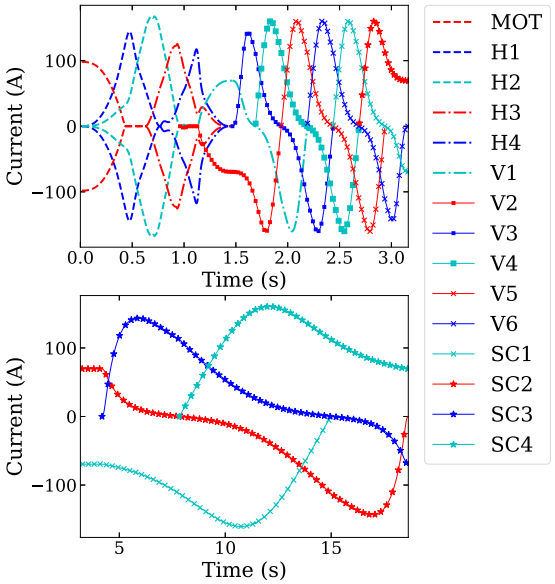

FIG. 4. Actual current profiles as a function of time. The last of the three transport sections is plotted separately with a different timescale.

sections. Each of them has initial and final velocity, as well as acceleration set to zero. The first horizontal section ends at 33 cm from the MOT chamber and the optimized velocity in this segment is 50 cm/s (see Fig. 3). After a 90° turn, the vertical path begins and is divided in two sections. The first vertical section extends to a total of 63 cm, of which the last 7.5 cm is inside the cryostat at 50-K temperature. The optimized maximum speed is 20 cm/s. After the first vertical section, the residual eddy currents in the segmented cryogenic shields greatly affect the transport efficiency at high velocities. This has been solved by sufficiently slowing the motion of the atoms for the remaining vertical path, benefiting from their long lifetime at cold environmental temperature (see Sec. IV). Therefore, in the last section, which is 10 cm long (making the total vertical length 73 cm), the atoms travel at a speed of 0.7 cm/s and have a negligible acceleration compared to the previous sections, as can be seen in the inset of the lower part of Fig. 3. This brings the total transport duration to approximately 18 s. These motion profiles have been obtained through optimization of the transport efficiency (see Sec. IV). In Fig. 4 the current pulses for each coil are plotted in time. For clarity, as in Fig. 3, the last section has been separated due to the long duration.

After the atoms have been transported in the cryogenic environment we can measure the lifetime of the atomic cloud.

IV. RESULTS

Initially, we choose a set of equations of motion to start the optimization procedure of the transport. The cloud accelerates out of the MOT chamber into the transport tube at a distance of 20 cm. Afterwards, it decelerates for the next 12 cm of the horizontal transport. Upon start of the transport, the magnetic trap current will be ramped down in 400-ms steps, while increasing the currents in the transport coils. The trap minimum will begin to move in the transport direction.

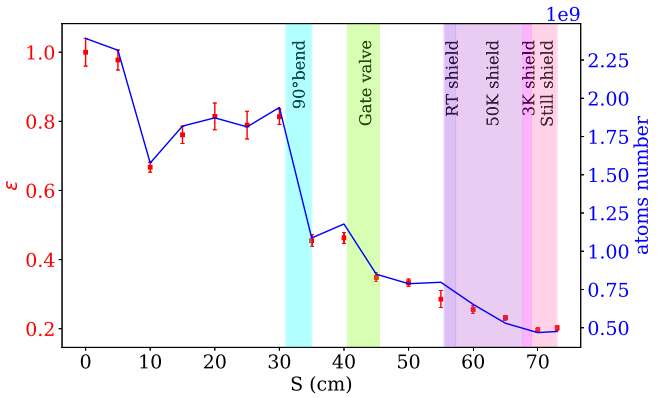

FIG. 5. Efficiency ϵ of the transport on the left axis and transported atomic population on the right axis.

We define the efficiency parameter of the transport as $\epsilon^2 = N_{t_{\rm cut}}/N_t$, where N_t is the atom number in the initial magnetic trap, and $N_{t_{\rm cut}}$ is the number of atoms after back and forth transport to an arbitrary position at the time $t_{\rm cut}$. The returning cloud from the transport is characterized in the MOT chamber with fluorescence imaging. The efficiency is defined as the fraction of cloud remaining after the forward transport, and hence it is squared for a two-way transport.

In Fig. 5 we plot the ϵ as a function of transport distance corresponding to certain $t_{\rm cut}$ values. We can observe three unusual dips in the efficiency, around 10, 30, and 40 cm. The explanation is the following: at 10 cm we have the maximum acceleration value of the first section and by reverting the motion, for the measurement in the MOT chamber, we expect a major loss. At 32 cm we are stopping the atoms before starting the vertical transport. At this location the measured trap lifetime is 2 s and therefore the cloud experiences increased background loss. Finally, at 40 cm we have a gate valve with a residual magnetization, and although it is degaussed periodically we still have losses there due to the distortion of the trapping magnetic field. The final atom number at the millikelvin stage is 5×10^8.

For further characterization of the cloud inside the still shield, we installed a laser beam with 260-μW power on one side of the cryostat and a CCD camera exposing 450 μs on the opposite side to perform absorption imaging. By evaluating the atom number for increasing holding times in the trap, one can estimate the lifetime from the inverse of the exponential decay Γ in Fig. 6. The measurements have been acquired at the 70-mK stage through the viewports and at the 50-K stage by reverting the motion of the atoms back into the MOT chamber, since there are no windows at this stage. The lifetime at the 50-K stage is 27 s, limited by the background pressure. At the 70-mK stage the lifetime increased to 13 min.

We note that the lifetime was enhanced from below 10 min to 13 min by applying a low-pass filter in the drive of the coils ($R = 1\ \Omega$, $C = 30\ \mu$F, $f_{\rm cut} = 5$ kHz) to prevent electrical noise. In addition, we improved the vacuum pressure between the room-temperature shield and the 50-K shield by installing nonevaporable getters and baking the outer shield of the cryostat prior to cooldown. We expect a negligible desorption from the millikelvin surfaces, which includes the

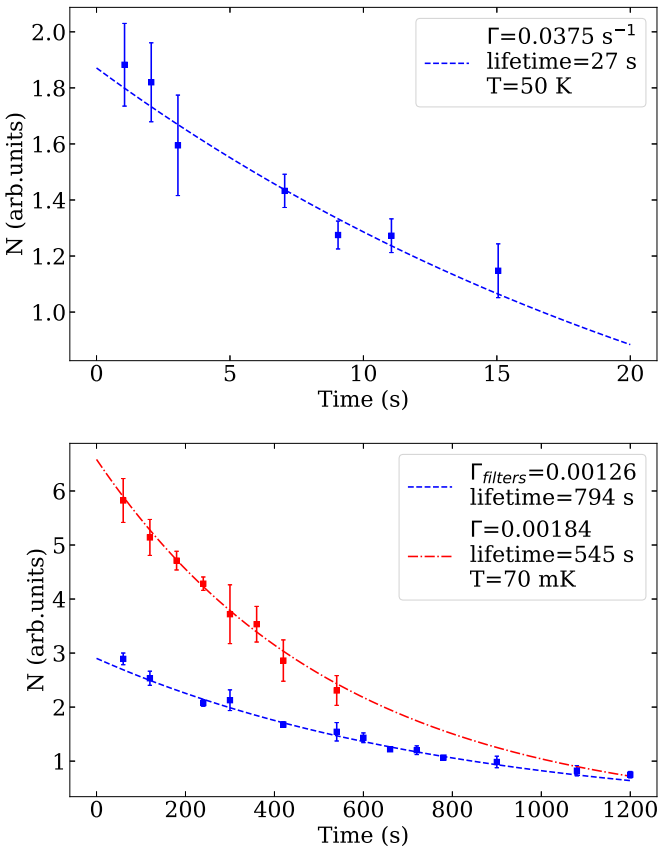

FIG. 6. Γ decay measurements of the trap. The number of atoms in trap N is shown on the y axis. In the upper plot, the atoms are held at the 50-K stage. In the lower one, atoms are held at 70 mK. The lifetime has been acquired with the superconducting coils current unfiltered and low-pass filtered. There is a noticeable improvement when filtered.

70-mK plate and the still shield. Furthermore, with closed shutters and viewports light-induced atom desorption is not present, as suggested as a limiting factor in [56].

From the decay Γ of the atomic cloud, the estimated pressure inside the still shield is $P = 2.55\times10^{-13}$ mbar. We report the model of the elastic collisions in the Appendix.

V. CONCLUSIONS

In conclusion, we demonstrated an experimental platform for hybrid quantum systems, which is capable of combining ultracold atom and superconducting circuit physics in a single setup. We showed that we can routinely transfer clouds of 5×10^8 atoms close to the millikelvin stage of a dilution refrigerator, at a base temperature of 70 mK. Lifetime measurements of the atomic cloud inside the cryogenic environment showed values of 13 min, which is a record in atomic physics experiments. This long lifetime gives us access to employ the ultracold atoms as an extremely sensitive probe for detecting static and fluctuating electric and magnetic fields. In future, we intend to use this setup to study interfaces between ultracold atoms and superconducting circuits. Different schemes for the merging and coupling of both systems are in preparation.

APPENDIX: SCATTERING THEORY OF BACKGROUND GAS COLLISIONS

The elastic collisions between the alkali-metal atoms and the surrounding gases make the atoms escape the trapping potential, defining the lifetime. The loss coefficient can be generally expressed as [57–59]

$$\Gamma = \sum_i n_i \langle \sigma v \rangle_{X,i}, \tag{A1}$$

where n_i is the density of the ith background species, X is the trapped species, and the velocity-averaged loss cross section $\langle \sigma v \rangle$ is a function of the trap depth $U_{\rm trap}$. If we consider the elastic scattering of an alkali-metal atom and a scattering particle, the change in kinetic energy of the atom is defined by

$$\Delta E \simeq \frac{\mu^2}{M_a} |\vec{v}_r|^2 (1 - \cos\theta), \tag{A2}$$

where μ is the reduced mass of the system, M_a is the mass of the atom alone, θ is the collision angle, and $\vec{v}_r = \vec{v}_a - \vec{v}_b$ is the initial relative velocity between the particles, with b being the background species. ΔE exceeds the trap depth for a minimum angle θ:

$$\theta_{\rm min} = \arccos\left(1 - \frac{M_a U_{\rm trap}}{\mu^2 |\vec{v}_r|^2}\right). \tag{A3}$$

The differential scattering cross section is defined as $d\sigma/d\Omega$, and it is equivalent to the quantum-mechanical scattering amplitude $|f(k,\theta)|^2$, by using the continuity equation for the wave function and the probability current density. For an incident scattering particle with wave number k, the cross section for loss-inducing collision from a trap of depth $U_{\rm trap}$ is

$$\sigma_{\rm loss} = \int_{\theta_{\rm min}}^{\pi} 2\pi \sin\theta |f(k,\theta)|^2 d\theta. \tag{A4}$$

By solving for the velocity average over the Maxwell-Boltzmann distribution one can obtain [58,60]

$$\langle \sigma v \rangle = \left(\frac{M_b}{2\pi k_b T}\right)^{3/2} \int_0^{\infty} 4\pi \sigma_{\rm loss}(k) v_b^3 e^{-M_b v_b^2/2k_b T} dv_b, \tag{A5}$$

where it is assumed that the atom is steady, $\vec{v}_r \simeq \vec{v}_b$, and $k = \mu v_b/\hbar$ and $\sigma_{\rm loss}$ contain the spherical harmonics.

It can be seen in [61,62] that we can further simplify the problem, obtaining

$$\gamma_i \approx 6.8 \frac{P_i}{(k_B T)^{2/3}} \left(\frac{C_i}{M_b}\right)^{1/3} (U_{\rm trap} M_a)^{-1/6}, \tag{A6}$$

where $\Gamma = \sum_i \gamma_i$ and C_i are the species dependent van der Waals coefficients estimated with the Slater-Kirkwood formula, which for helium is equal to 35 in atomic units [61,63,64]. P_i represents the partial pressure, T represents the background gas temperature, and mass M_b and M_a represent the rubidium mass. We must note that the trap depth $U_{\rm trap}$ varies with the laser and magnetic trap parameters and can be challenging to quantify, usually varying between 0.5 and 2 K [58,65], but with a weak dependence in γ_i. At the considered temperatures, only helium atoms contribute to the background gas vapor pressure. Following the above considerations, one can estimate the parameter $\Gamma/P = 4.93 \times 10^9$ mbar^{-1} s^{-1} for collisions between ground-state Rb atoms

and helium-4 at a background temperature of $T = 0.07$ K and $U_{\text{trap}} \approx 1$ K. Using Eq. (A6) and substituting the exponential decay Γ of the cloud in the magnetostatic trap in the cryostat from Fig. 6, we obtain a pressure of $P = 2.55\times10^{-13}$ mbar, below the one reported at 3.6-K temperature in [56], which has a nearly 10-min lifetime.

[1] T. Yamamoto, Y. A. Pashkin, O. Astafiev, Y. Nakamura, and J. S. Tsai, Nature (London) **425**, 941 (2003).

[2] D. Leibfried, B. DeMarco, V. Meyer, D. Lucas, M. Barrett, J. Britton, W. M. Itano, B. Jelenkovic, C. Langer, T. Rosenband, and D. J. Wineland, Nature (London) **422**, 412 (2003).

[3] L. DiCarlo, J. M. Chow, J. M. Gambetta, L. S. Bishop, B. R. Johnson, D. I. Schuster, J. Majer, A. Blais, L. Frunzio, S. M. Girvin, and R. J. Schoelkopf, Nature (London) **460**, 240 (2009).

[4] T. Monz, P. Schindler, J. T. Barreiro, M. Chwalla, D. Nigg, W. A. Coish, M. Harlander, W. Hänsel, M. Hennrich, and R. Blatt, Phys. Rev. Lett. **106**, 130506 (2011).

[5] E. Lucero, R. Barends, Y. Chen, J. Kelly, M. Mariantoni, A. Megrant, P. O'Malley, D. Sank, A. Vainsencher, J. Wenner, T. White, Y. Yin, A. N. Cleland, and J. M. Martinis, Nat. Phys. **8**, 719 (2012).

[6] M. Veldhorst, C. H. Yang, J. C. C. Hwang, W. Huang, J. P. Dehollain, J. T. Muhonen, S. Simmons, A. Laucht, F. E. Hudson, K. M. Itoh, A. Morello, and A. S. Dzurak, Nature (London) **526**, 410 (2015).

[7] K. Kim, M. S. Chang, S. Korenblit, R. Islam, E. E. Ed-wards, J. K. Freericks, G. D. Lin, L. M. Duan, and C. Monroe, Nature (London) **465**, 590 (2010).

[8] J. Simon, W. S. Bakr, R. Ma, M. E. Tai, P. M. Preiss, and M. Greiner, Nature (London) **472**, 307 (2011).

[9] R. Blatt and C. F. Roos, Nat. Phys. **8**, 277 (2012).

[10] I. Bloch, J. Dalibard, and S. Nascimbene, Nat. Phys. **8**, 267 (2012).

[11] A. A. Houck, H. E. Türeci, and J. Koch, Nat. Phys. **8**, 292 (2012).

[12] I. M. Georgescu, S. Ashhab, and F. Nori, Rev. Mod. Phys. **86**, 153 (2014).

[13] R. Barends, L. Lamata, J. Kelly, L. García Álvarez, A. G. Fowler, A. Megrant, E. Jeffrey, T. C. White, D. Sank, J. Y. Mutus, B. Campbell, Y. Chen, Z. Chen, B. Chiaro, A. Dunsworth, I.-C. Hoi, C. Neill, P. J. J. O'Malley, C. Quintana, P. Roushan, A. Vainsencher, J. Wenner, E. Solano, and J. M. Martinis, Nat. Commun. **6**, 7654 (2015).

[14] L. M. Duan, M. D. Lukin, J. I. Cirac, and P. Zoller, Nature (London) **414**, 413 (2001).

[15] R. Ursin, F. Tiefenbacher, T. Schmitt-Manderbach, H. Weier, T. Scheidl, M. Lindenthal, B. Blauensteiner, T. Jennewein, J. Perdigues, P. Trojek, B. Ömer, M. Fürst, M. Meyenburg, J. Rarity, Z. Sodnik, C. Barbieri, H. Weinfurter, and A. Zeilinger, Nat. Phys. **3**, 481 (2007).

[16] N. Gisin and R. Thew, Nat. Photon. **1**, 165 (2007).

[17] C. L. Degen, F. Reinhard, and P. Cappellaro, Rev. Mod. Phys. **89**, 035002 (2017).

[18] M. Saffman, T. G. Walker, and K. Mølmer, Rev. Mod. Phys. **82**, 2313 (2010).

[19] M. H. Devoret and R. J. Schoelkopf, Science **339**, 1169 (2013).

[20] J. L. O'Brien, A. Furusawa, and J. Vučković, Nat. Photon. **3**, 687 (2009).

[21] R. J. Schoelkopf and S. M. Girvin, Nature (London) **451**, 664 (2008).

[22] M. Wallquist, K. Hammerer, P. Rabl, M. Lukin, and P. Zoller, Phys. Scr. **2009**, 014001 (2009).

[23] Z. L. Xiang, S. Ashhab, J. Q. You, and F. Nori, Rev. Mod. Phys. **85**, 623 (2013).

[24] R. Barends, J. Kelly, A. Megrant, A. Veitia, D. Sank, E. Jeffrey, T. C. White, J. Mutus, A. G. Fowler, B. Campbell, Y. Chen, Z. Chen, B. Chiaro, A. Dunsworth, C. Neill, P. O'Malley, P. Roushan, A. Vainsencher, J. Wenner, A. N. Korotkov, A. N. Cleland, and J. M. Martinis, Nature (London) **508**, 500 (2014).

[25] P. V. Klimov, J. Kelly, Z. Chen, M. Neeley, A. Megrant, B. Burkett, R. Barends, K. Arya, B. Chiaro, Y. Chen, A. Dunsworth, A. Fowler, B. Foxen, C. Gidney, M. Giustina, R. Graff, T. Huang, E. Jeffrey, E. Lucero, J. Y. Mutus, O. Naaman, C. Neill, C. Quintana, P. Roushan, D. Sank, A. Vainsencher, J. Wenner, T. C. White, S. Boixo, R. Babbush, V. N. Smelyanskiy, H. Neven, and J. M. Martinis, Phys. Rev. Lett. **121**, 090502 (2018).

[26] G. Wendin, Rep. Prog. Phys. **80**, 106001 (2017).

[27] S. Bernon, H. Hattermann, D. Bothner, M. Kufinke, P. Weiss, F. Jessen, D. Cano, M. Kemmler, R. Kleiner, D. Koelle, and J. Fortágh, Nat. Commun. **4**, 2380 (2013).

[28] J. I. Cirac, P. Zoller, H. J. Kimble, and H. Mabuchi, Phys. Rev. Lett. **78**, 3221 (1997).

[29] H. Hattermann, D. Bothner, L. Y. Ley, B. Ferdinand, D. Wiedmaier, L. Sárkány, R. Kleiner, D. Koelle, and J. Fortágh, Nat. Commun. **8**, 2254 (2017).

[30] M. F. Brandl, M. W. van Mourik, L. Postler, A. Nolf, K. Lakhmanskiy, R. R. Paiva, S. Möller, N. Daniilidis, H. Häffner, V. Kaushal, T. Ruster, C. Warschburger, H. Kaufmann, U. G. Poschinger, F. Schmidt-Kaler, P. Schindler, T. Monz, and R. Blatt, Rev. Sci. Instrum. **87**, 113103 (2016).

[31] S. Minniberger, F. Diorico, S. Haslinger, C. Hufnagel, C. Novotny, N. Lippok, J. Majer, C. Koller, S. Schneider, and J. Schmiedmayer, Appl. Phys. B **116**, 1017 (2014).

[32] T. Mukai, C. Hufnagel, A. Kasper, T. Meno, A. Tsukada, K. Semba, and F. Shimizu, Phys. Rev. Lett. **98**, 260407 (2007).

[33] A. Emmert, A. Lupaşcu, M. Brune, J.-M. Raimond, S. Haroche, and G. Nogues, Phys. Rev. A **80**, 061604(R) (2009).

[34] A. Emmert, A. Lupaşcu, G. Nogues, M. Brune, J.-M. Raimond, and S. Haroche, Eur. Phys. J. D **51** 173 (2009).

[35] M. Siercke, K. S. Chan, B. Zhang, M. Beian, M. J. Lim, and R. Dumke, Phys. Rev. A **85**, 041403(R) (2012).

[36] G. Pagano, P. W. Hess, H. B. Kaplan, W. L. Tan, P. Richerme, P. Becker, A. Kyprianidis, J. Zhang, E. Birckelbaw, M. R. Hernandez, Y. Wu, and C. Monroe, Quantum Sci. Technol. **4**, 014004 (2018).

[37] M. Stammeier, S. Garcia, T. Thiele, J. Deiglmayr, J. A. Agner, H. Schmutz, F. Merkt, and A. Wallraff, Phys. Rev. A **95**, 053855 (2017).

[38] M. Stammeier, S. Garcia, and A. Wallraff, Quantum Sci. Technol. **3**, 045007 (2018).
[39] D. Yu, L. C. Kwek, L. Amico, and R. Dumke, Quantum Sci. Technol. **2**, 035005 (2017).
[40] D. Yu, L. C. Kwek, L. Amico, and R. Dumke, Phys. Rev. A **95**, 053811 (2017).
[41] D. Yu, A. Landra, M. M. Valado, C. Hufnagel, L. C. Kwek, L. Amico, and R. Dumke, Phys. Rev. A **94**, 062301 (2016).
[42] D. Yu, M. M. Valado, C. Hufnagel, L. C. Kwek, L. Amico, and R. Dumke, Sci. Rep. **6**, 38356 (2016).
[43] D. Yu, M. M. Valado, C. Hufnagel, L. C. Kwek, L. Amico, and R. Dumke, Phys. Rev. A **93**, 042329 (2016).
[44] K. R. Patton and U. R. Fischer, Europhys. Lett. **102**, 20001 (2013).
[45] K. R. Patton and U. R. Fischer, Phys. Rev. A **87**, 052303 (2013).
[46] K. R. Patton and U. R. Fischer, Phys. Rev. Lett. **111**, 240504 (2013).
[47] Z. Kim, C. P. Vlahacos, J. E. Hoffman, J. A. Grover, K. D. Voigt, B. K. Cooper, C. J. Ballard, B. S. Palmer, M. Hafezi, J. M. Taylor, J. R. Anderson, A. J. Dragt, C. J. Lobb, L. A. Orozco, S. L. Rolston, and F. C. Wellstood, AIP Adv. **1**, 042107 (2011).
[48] M. Hafezi, Z. Kim, S. L. Rolston, L. A. Orozco, B. L. Lev, and J. M. Taylor, Phys. Rev. A **85**, 020302(R) (2012).
[49] D. Yu and R. Dumke, Phys. Rev. A **97**, 053813 (2018).
[50] D. Yu, A. Landra, L. C. Kwek, L. Amico, and R. Dumke, New J. Phys. **20**, 023031 (2018).
[51] L. Chin Chean, Transport and interaction of Rb 87 atoms in a dilution fridge, Ph.D. thesis, Centre for Quantum Technologies, National University of Singapore, 2018.
[52] H. J. Lewandowski, D. M. Harber, D. L. Whitaker, and E. A. Cornell, J. Low Temp. Phys. **132**, 309 (2003).
[53] K. Nakagawa, Y. Suzuki, M. Horikoshi, and J. Kim, Appl. Phys. B **81**, 791 (2005).
[54] M. Greiner, I. Bloch, T. W. Hänsch, and T. Esslinger, Phys. Rev. A **63**, 031401(R) (2001).
[55] S. Haslinger, Cold atoms in a cryogenic environment, Ph.D. thesis, Vienna University of Technology, 2011.
[56] P. A. Willems and K. G. Libbrecht, Phys. Rev. A **51**, 1403 (1995).
[57] S. Bali, K. M. O'Hara, M. E. Gehm, S. R. Granade, and J. E. Thomas, Phys. Rev. A **60**, R29(R) (1999).
[58] J. Van Dongen, C. Zhu, D. Clement, G. Dufour, J. L. Booth, and K. W. Madison, Phys. Rev. A **84**, 022708 (2011).
[59] S. Eckel, D. S. Barker, J. A. Fedchak, N. N. Klimov, E. Norrgard, J. Scherschligt, C. Makrides, and E. Tiesinga, Metrologia **55**, S182 (2018).
[60] J. Van Dongen, Study of background gas collisions in atomic traps, Ph.D. thesis, University of British Columbia, 2014.
[61] T. Arpornthip, C. A. Sackett, and K. J. Hughes, Phys. Rev. A **85**, 033420 (2012).
[62] J. E. Bjorkholm, Phys. Rev. A **38**, 1599 (1988).
[63] H. Margenau and N. Kestner, in *Theory of Intermolecular Forces*, 2nd ed., International Series in Natural Philosophy Vol. 18 (Pergamon Press, New York, 1969).
[64] T. M. Miller and B. Bederson, in *Advances in Atomic and Molecular Physics*, edited by D. Bates and B. Bederson (Academic Press, New York, 1978), Vol. 13, pp. 1–55.
[65] S. D. Gensemer, V. Sanchez-Villicana, K. Y. N. Tan, T. T. Grove, and P. L. Gould, Phys. Rev. A **56**, 4055 (1997).